


# Feasibility study to investigate diffusion of Fe in Si using a Mössbauer spectroscopic microscope

Y. Yoshida<sup>1</sup>  · Y. Ino<sup>1</sup> · K. Matsumuro<sup>1</sup> ·  
T. Watanabe<sup>1</sup> · H. Fujita<sup>1</sup> · K. Hayakawa<sup>1</sup> · K. Yukihiro<sup>1</sup> ·  
K. Ogai<sup>2</sup> · K. Moriguchi<sup>2</sup> · Y. Harada<sup>2</sup> · H. Soejima<sup>1</sup>

Published online: 1 September 2016  
© Springer International Publishing Switzerland 2016

**Abstract** A prototype Mössbauer Spectroscopic Microscope is applied for the feasibility study of  $^{57}\text{Fe}$  impurity diffusion in Si wafers. A 2nm- $^{57}\text{Fe}$  deposited Si wafer is annealed at 430 °C for 1 hour, and subsequently the 1/3 area of the wafer is further grinded with an angle of 6 degrees to the original surface to get a higher depth resolution for the mapping. Subsequently, the mapping images for  $\text{Fe}_{\text{sub}}^0$ ,  $\text{Fe}_{\text{int}}^0$ , and  $\text{Fe}_{\text{int}}^+$  states are measured separately for the two different areas: one area (A) along the grinded surface, and the other (B) along the original wafer surface crossing through the  $^{57}\text{Fe}$ -deposition boundary. By integrating the mapping intensity the diffusivity of each Fe component along the two different directions can be evaluated and compared with an average Fe diffusivity in Si, which is measured by EDS mapping data obtained for the same area.

**Keywords** Mössbauer spectroscopic microscope · Fe diffusion in Si

## 1 Introduction

Recently, direct observation on atomic diffusion is essential to control and improve material characteristics on an atomistic scale. Immediately after the discovery of the Mössbauer effect in 1958, Singwi and Sjölander [1] predicted theoretically in 1960 that a Mössbauer spectrum  $\sigma(\mathbf{k}, \omega)$  can be described as a space-time Fourier transformation of a

---

This article is part of the Topical Collection on *Proceedings of the International Conference on Hyperfine Interactions and their Applications (HYPERFINE 2016)*, Leuven, Belgium, 3-8 July 2016

---

✉ Y. Yoshida  
yoshida.yutaka@sist.ac.jp

<sup>1</sup> Shizuoka Institute of Science and Technology, Toyosawa 2200-2,  
Fukuroi City, Shizuoka 437-8555, Japan

<sup>2</sup> APCO.Ltd., Kitano-cho 522-10, Hachioji 192-0906, Tokyo, Japan

self-correlation function  $G_s(\mathbf{R}, t)$ , and therefore, the atomic jumps within the lifetime can be directly observed as a line broadening of the spectrum.

$$\sigma(\mathbf{k}, \omega) = f Re \frac{1}{\pi \hbar} \int_{-\infty}^{\infty} \exp[-i(\omega - \omega_0)t - \frac{\Gamma_0 t}{2\hbar}] \sum_j \exp(i\mathbf{k} \cdot \mathbf{R}_j) G(\mathbf{R}_j, t) dt$$

Based on their prediction, many groups tried to observe the broadenings, and to interpret the experimental results in terms of the jump models. At the early stage, however, there remained still a large discrepancy between the “tracer diffusivity” obtained from a radioactive tracer experiment and the “Mössbauer diffusivity” from a line broadening of Mössbauer spectrum. To know the historical development until early 1980’, we refer the following publications by Chudley and Elliot [2], Dibar-Ure and Flinn [3], Wolf [4], Mullen [5], Mantl, Petry, Schroeder and Vogl [6], Nowik, Cohen and Bauminger [7, 8], and Dattagupta [9].

At the Hahn-Meitner Institute Berlin, a “high temperature UHV-furnace” was developed in the middle of 1980’, and was applied for the study on the self-diffusion of pure Fe via thermal vacancies: The Mössbauer spectra were successfully measured in both the  $\gamma$ - and  $\delta$ -phases up to 1740 K [10], and finally shown that the Mössbauer diffusivities reduced from the line broadenings agreed well with the values of the tracer diffusivities. This was the first clear experimental proof that Mössbauer spectroscopy is able to provide the atomistic information on the long-range self-diffusion based on the Singwi and Sjölander theory. For a fast impurity diffusion of Fe in metals and in semiconductors [11], on the other hands, where an interstitial diffusion mechanism was expected, an in-beam experimental set-up, which combined Coulomb-excitation with a recoil-implantation technique, was constructed at a VICKSI heavy ion accelerator to study the fast diffusion of Fe in  $\alpha$ -Zr [12] and Alkaline metals [13], and later in Si [14]: A local jump process of  $^{57}\text{Fe}$  atom (i.e. cage motion) on interstitial sites in  $\alpha$ -Zr were clearly detected at about 50 K in terms of a sudden area decrease accompanied with a quadrupole relaxation [12], while a long-range interstitial diffusion of Fe in Si was detected at about 500 K in terms of the line broadenings [14]. At CERN-ISOLDE, the line broadenings of interstitial Fe in Si were also observed at around 500 K in an on-line  $^{57}\text{Mn}$  implantation experiments [15]. Furthermore, GeV- $^{57}\text{Mn}$  beam was extracted via an on-line projectile fragment separator at RIKEN, and was subsequently implanted into Si wafers: interstitial and substitutional  $^{57}\text{Fe}$  diffusion could be followed as the line broadenings and the relaxation of two corresponding components [16].

All the experimental results [2–7, 9–15] mentioned above were obtained in homogeneous solids mainly, and the diffusion lengths and times characteristic for the self-correlation function were considered to be up to a few nanometers and  $10^{-6}$  to  $10^{-8}$  s, respectively. When we consider to measure diffusion in a material, however, we notice the material contains always inhomogeneity, i.e., microstructures, which must influence and change the diffusivities in the microstructures: for instance, multi-crystalline Si solar cells contain crystal grains, dislocations, precipitations and lattice defects [17], and the diffusion of Fe impurities must be strongly influenced by internal stress fields originated from such microstructures. The Fe impurities are considered to be strong trapping sites of electrical carriers created by the sun light, leading a low efficiency of the solar cells, and therefore, it is inevitable to control the diffusion and segregation of Fe impurities in mc-Si wafer during the production processes [17]. This indicates clearly that a new methodology must be developed for controlling the microstructures.

Here we report the first results from the study on Fe diffusion in Si wafer using “Mössbauer spectroscopic microscope (MSM)”, which enables us to measure the Fe diffusion profiles separately for different Fe states in Si with a spatial sensitivity of several micrometres. This new method provides a possibility to investigate the diffusion processes by taking into account of the interactions and the correlations between Fe impurities and lattice defects such as dislocations, grain boundaries, and residual stresses in different grains.

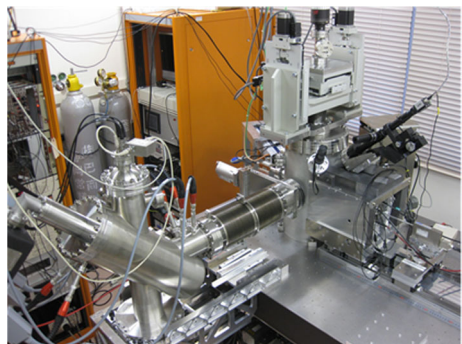
## 2 Mössbauer spectroscopic microscope (MSM)

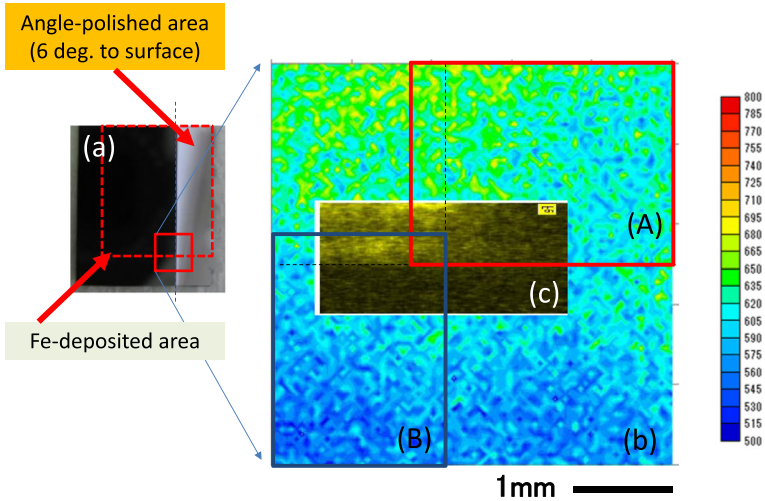
A prototype set-up (Fig. 1) of “Mössbauer Spectroscopic Microscope (MSM)” has been recently built and completed in our group [18, 19], combining with different evaluation equipment such as a scanning electron microscope (SEM), an electron beam induced current (EBIC), an energy dispersive X-ray spectrometer (EDS), an electron backscatter diffraction (EBSD), and a cylindrical sector electron analyser (FOCUS, HV-CSA). We use a multi-capillary X-ray (MCX) lens to focus 14.4keV  $\gamma$ -rays on a sample which is mounted on a precision XYZ- $\theta$  stage. The electrons and transmitted  $\gamma$ -rays are measured as function of the sample position by a funnel type-MCP detector and a Si-PIN diode detector, respectively. 3.7GBq- $^{57}\text{Co}$  source is mounted on a linear motion driver operated with a constant Doppler velocity corresponding to the isomer shift of a Mössbauer spectral component, enabling us a mapping of each Fe component selectively with a spatial sensitivity of several micrometres.

## 3 Experimental procedure

A CZ-Si wafer ( $10^{15} \text{ B/cm}^3$ ) was cut into a square plate of  $30 \text{ mm} \times 30 \text{ mm} \times 500 \mu\text{m}$ . After removing a natural oxide layer by 5%-HF, 2nm-thick  $^{57}\text{Fe}$  was deposited in an area of  $10 \text{ mm} \times 10 \text{ mm}$  on the wafer, which is shown in Fig. 2a, and subsequently annealed at  $430^\circ$  for 1 hour in a vacuum furnace. Mössbauer spectrum was measured in air at room temperature. Furthermore, about 1/3 of the sample on the right hand side was angle-polished with an angle of 6 degrees to the surface, as is seen in Fig. 2a. Finally, three mapping images of conversion and Auger electrons due to Mössbauer effect were measured as function of

**Fig. 1** Mössbauer spectroscopic microscope (MSM)

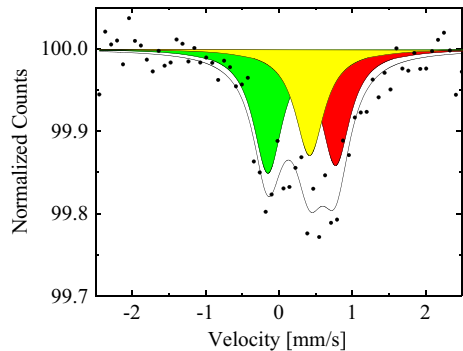




**Fig. 2** a  $^{57}\text{Fe}$ -deposited Si wafer, and  $^{57}\text{Fe}$ -deposited area is shown by red broken-line rectangular, b MSM mapping for red-line square area in Fig. 1a, c EDS mapping of Fe- $L_{\alpha 1}$  X-ray. The mapping areas of (A) and (B), which are shown in Fig. 1b, are evaluated for the  $^{57}\text{Fe}$  diffusivities along the angle-polished area and along the surface crossing through the  $^{57}\text{Fe}$ -deposition boundary, respectively

sample position by adjusting the resonant absorption conditions of 14.4keV- $\gamma$ -rays corresponding to different spectral components, i.e., substitutional  $\text{Fe}_{\text{sub}}^0$ , and interstitials  $\text{Fe}_{\text{int}}^0$  and  $\text{Fe}_{\text{int}}^+$ , respectively. We accumulated the electrons and the  $\gamma$ -rays simultaneously for 35 s at  $80 \times 80$  points with a mapping step of  $50 \mu\text{m}$ . The focal distance and size of the Multi-capillary X-ray lens was 50 mm and  $250 \mu\text{m}\phi$ , respectively, for the whole experiments. In order to compare the diffusivity of Fe in Si reported so far [20], two different areas were evaluated: one area (A) along the grinded surface, and the other (B) along the original wafer surface crossing through the  $^{57}\text{Fe}$ -deposition boundary. By integrating the mapping intensity of the electrons, the diffusivity of each Fe component along two different directions could be evaluated and compared with the total Fe diffusivity in Si, which was measured by EDS mapping of Fe- $L_{\alpha 1}$  X-ray obtained for the area presented in Fig. 2c.

**Fig. 3** Mössbauer Spectrum of  $^{57}\text{Fe}$  deposited Si wafer, which was annealed at  $430 \text{ }^\circ\text{C}$



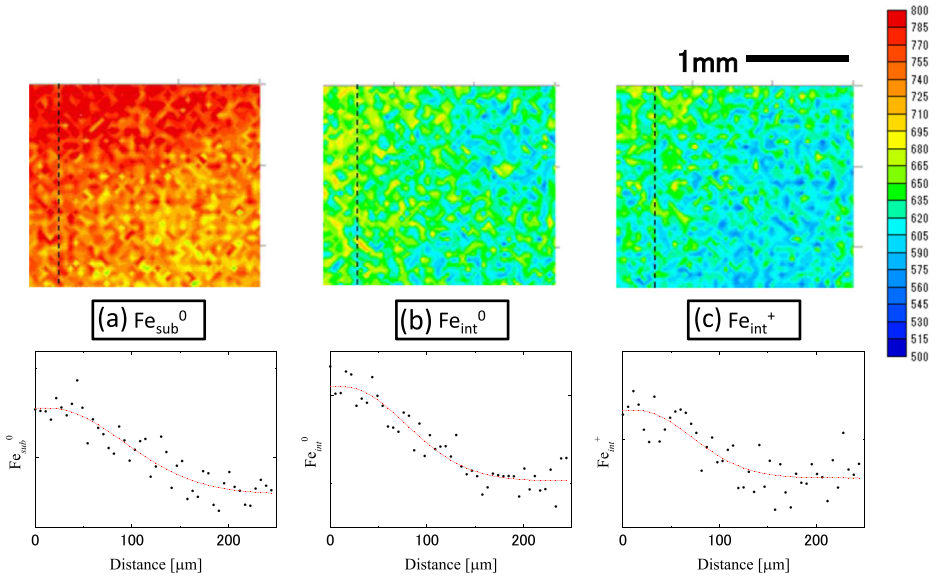


**Fig. 4** Three mapping images along angle-grinded surface, corresponding to different spectral components, i.e., (a) substitutional  $Fe_{sub}^0$ , and (b) interstitials  $Fe_{int}^0$  and (c) interstitial  $Fe_{int}^+$ , respectively. The diffusion profiles are plotted as function of depth, which is deduced by correcting the angle of 6 degrees

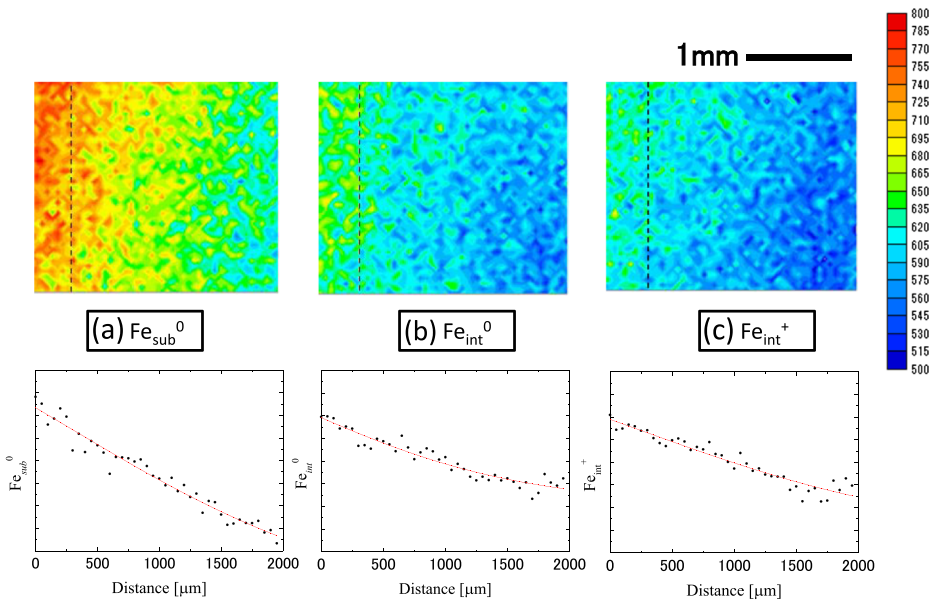


**Fig. 5** Three mapping images along the surface, corresponding to different spectral components, i.e., (a) substitutional  $Fe_{sub}^0$ , and (b) interstitials  $Fe_{int}^0$  and (c) interstitial  $Fe_{int}^+$ , respectively. The diffusion profiles are plotted as function of surface distance from the  $^{57}Fe$ -deposited boundary

**Table 1** Diffusivities of Fe in Si evaluated from the MSM mapping images.

Methods	Diffusion profiles	Fe states	$D / \text{cm}^2\text{s}^{-1}$	
EDS	depth	total	$8.0 \times 10^{-9}$	
	Parallel to surface		$1.1 \times 10^{-9}$	
MSM	depth	total	$5.7 \times 10^{-9}$	
		substitutional $\text{Fe}_{\text{sub}}^0$	$8.3 \times 10^{-9}$	
		interstitial $\text{Fe}_i^0$	$5.6 \times 10^{-9}$	
	Parallel to surface	interstitial $\text{Fe}_i^+$	$4.5 \times 10^{-9}$	
		total	$6.1 \times 10^{-6}$	
		substitutional $\text{Fe}_{\text{sub}}^0$	$7.4 \times 10^{-6}$	
		interstitial $\text{Fe}_i^0$	$4.4 \times 10^{-6}$	
interstitial $\text{Fe}_i^+$	$7.0 \times 10^{-6}$			
Reference	[20]	total	$1.7 \times 10^{-8}$	at 430°C

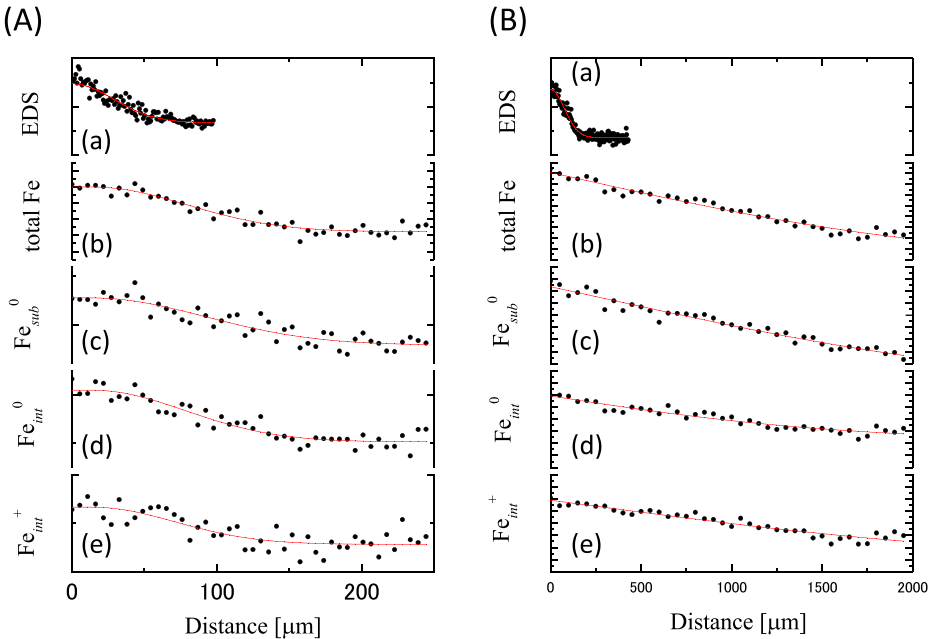
## 4 Results and discussions

Figure 3 shows Mössbauer spectrum of 2nm- $^{57}\text{Fe}$  deposited Si wafer ( $10^{15} \text{ B/cm}^3$ ) measured at room temperature after the annealing at 430°C for 1 hour. The spectrum can be fitted by the superposition of three Lorenz functions corresponding to substitutional  $\text{Fe}_{\text{s}}^0$ , and interstitial  $\text{Fe}_i^0$  and  $\text{Fe}_i^+$ . The isomer shifts of  $\text{Fe}_{\text{s}}^0$  (green) and  $\text{Fe}_i^+$  (red) are  $-0.15 \pm 0.03$  and  $+0.77 \pm 0.02 \text{ mm/s}$ , respectively. These values are in rather good agreement with those of  $-0.13$  and  $+0.67 \text{ mm/s}$  obtained theoretically by Wright et al. [21]. The isomer shift of neutral interstitial  $\text{Fe}_i^0$  (yellow), however, is  $0.42 \pm 0.05 \text{ mm/s}$ , which is different from that of the calculation,  $0.72 \text{ mm/s}$ . Our value of  $\text{Fe}_i^0$  is close to that of  $\text{FeV}_2$ ,  $0.39 \text{ mm/s}$ , in their calculation. There remains still some problems in the assignments of the Fe components in Si. In the following, we use our assignment to discuss the diffusivities.

### 4.1 $^{57}\text{Fe}$ Fe diffusion profile along the angle-polished area

Three mapping images of conversion and Auger electrons due to Mössbauer effect were measured by adjusting the Doppler velocities of  $^{57}\text{Co}$  source, i.e., the resonant absorption conditions of 14.4keV- $\gamma$ -rays corresponding to different spectral components, i.e., (a) substitutional  $\text{Fe}_{\text{sub}}^0$ , and (b) interstitials  $\text{Fe}_{\text{int}}^0$  and (c) interstitial  $\text{Fe}_{\text{int}}^+$ , respectively. The mapping images are shown in Fig. 4a, b and c, respectively. The same colouring scale is used for all images between 500 and 800 counts/mapping point. The broken line on the left-hand side of each mapping indicates the position of the surface deposited with  $^{57}\text{Fe}$ . After the diffusion annealing at 430°C for one hour, the  $^{57}\text{Fe}$  diffusion profiles of Fig. 4a, b and c appear to be different each other, suggesting different diffusivities for different Fe states in Si. The mapping intensity is essentially proportional to the number of the Fe atoms distributing in the region down to about 100 nm below the surface, from where the electrons can be emitted.

The average intensity of Fig. 4a is clearly higher than those of Fig. 4b and c. This might be due to the depth distribution of substitutional  $\text{Fe}_{\text{sub}}^0$ . In addition, the mapping image might contain information on a density fluctuation of Fe atoms, which could be originated from the atomic correlations. For the simplicity, however, we will not be discussing on these problems. We will, therefore, analyse only the relative changes of the integrated mapping intensity as function of the distance from the surface. These 1D-diffusion profiles can be



**Fig. 6** **A** Diffusion profiles along the depth obtained from EDS mapping of (a) Fe-L $\alpha_1$  X-ray, MSM mappings of (b) total electron intensity, (c) substitutional Fe $_{sub}^0$ , (d) interstitials Fe $_{int}^0$  and (e) interstitial Fe $_{int}^+$ , respectively. **B** Diffusion profiles along the surface obtained from EDS mapping of (a) Fe-L $\alpha_1$  X-ray, MSM mappings of (b) total electron intensity, (c) substitutional Fe $_{sub}^0$ , (d) interstitials Fe $_{int}^0$  and (e) interstitial Fe $_{int}^+$ , respectively

obtained by summing up the counts along the direction perpendicular to the depth. By taking into account of 6 degrees, i.e., the angle between the grinding plane and the surface, we can estimate the diffusion depth. Accordingly, the diffusivity for each Fe component can be deduced as function of depth from the surface by assuming a simple Gaussian distribution. The total diffusivity of all Fe components is evaluated as  $5.7 \times 10^{-9}$  cm $^2$ /s, the value of which is close to those obtained from the EDS mapping image,  $8.0 \times 10^{-9}$  and  $1.7 \times 10^{-8}$  cm $^2$ /s from the reference [20]. The results are summarized in Table 1.

#### 4.2 $^{57}\text{Fe}$ diffusion profile along the surface crossing through the $^{57}\text{Fe}$ -deposition boundary

The mapping images along the surface and their diffusion profiles are shown in Fig. 5a, b and c, respectively. The broken line on the left hand side indicate the  $^{57}\text{Fe}$ -deposition boundary. The diffusivities are summarized in Table 1. Surprisingly seen is that the diffusivity along the surface is three orders of magnitude larger than that of along the depth, although the diffusivity estimated by the EDS mapping image shows only  $1.1 \times 10^{-9}$  cm $^2$ /s. This big discrepancy may be due to the detection range: 100nm for MSM and 300nm for EDS. Moreover, further investigation is necessary to clarify the problem. It should be noticed that there is oxygen distribution which coincides the  $^{57}\text{Fe}$ -deposition area. Accordingly, the experimental conditions must be also improved to clarify the problems of Fe diffusion and segregation in Si matrix.



Figure 6A and B show the summary on the diffusion profiles obtained for both direction, i.e., perpendicular and parallel to the Si surface, and the results are compared with those from the EDS mapping of Fe-L $\alpha$ 1-X-ray (Fig. 2c) as well as other references [20]. The diffusion profiles of the total Fe, (b) in Fig. 6A and B, are deduced from the sum of the Fe components, corresponding to (c) substitutional Fe<sub>sub</sub><sup>0</sup>, (d) interstitials Fe<sub>int</sub><sup>0</sup> and (e) interstitial Fe<sub>int</sub><sup>+</sup>, respectively. The sum profile is expected to be equivalent to the profile obtained by the EDS measurement. There appears, however, to exist a difference close to the surface in (A) and the deposition boundary in (B).

## 5 Summary

A new set-up of “Mössbauer Spectroscopic Microscope (MSM)” has been recently built and completed in our group. The mapping images of a <sup>57</sup>Fe-deposited and annealed Si wafer are compared in two different areas (A) and (B), indicating different diffusion profiles, which provides us a possibility to investigate the diffusion processes selectively for the different states of Fe atoms in Si matrix. This method can be also applied for the diffusion study of Fe in Si-solar cells, where the interactions and the correlations must be playing an important role between Fe impurities and lattice defects such as dislocations, grain boundaries, and residual stresses in different grains.

**Acknowledgments** This work was supported by “Development of Systems and Technologies for Advanced Measurement and Analysis” Program of Japan Science and Technology Agency (JST).

## References

1. Singwi, K.S., Sjölander, A.: *Phys. Rev.* **120**, 1093 (1960)
2. Chudley, C.T., Elliot, R.J.: *Proc. Phys. Soc. (London)* **77**, 353 (1961)
3. Dibbar-Ure, M.C., Flinn, P.A.: *Appl. Phys. Lett.* **23**, 587 (1973)
4. Wolf, D.: *Appl. Phys. Lett.* **30**, 617 (1977)
5. Mullen, J.G.: *Phys. Lett.* **79A**, 457 (1980). In *Proc. of ICAME1981*, Jaipur, 29 (1982)
6. Mantl, S., Petry, W., Schroeder, K., Vogl, G.: *Phys. Rev.* **27**, 5313 (1983)
7. Nowik, I., Cohen, S.G., Bauminger, E.R., Ofer, S.: *Phys. Rev. Lett.* **50**, 152 (1983)
8. Bauminger, E.R., Nowik, I.: In: Dickson, D.P.E., Berry, F.J. (eds.) *Mössbauer Spectroscopy*, p. 219. Cambridge University Press (1986)
9. Dattagupta, S.: In: Dickson, D.P.E., Berry, F.J. (eds.) *Mössbauer Spectroscopy*, p. 198. Cambridge University Press (1986)
10. Heiming, A., Steinmetz, K.H., Vogl, G., Yoshida, Y.: *J. Phys. F: Metal Phys.* **18**, 1491 (1988)
11. Langouche, G., Yoshida, Y.: *Ion Implantation in Mössbauer Spectroscopy-Tutorial Book*. In: Yoshida, Y., Langouche, G. (eds.) vol. 37. Springer (2012)
12. Yoshida, Y., Menningen, M., Sielemann, R., Vogl, G., Weyer, G., Schroeder, K.: *Phys. Rev. Lett.* **61**, 195 (1988)
13. Keck, B., Sielemann, R., Yoshida, Y.: *Phys. Rev. Lett.* **71**, 4178–4181 (1993)
14. Schwalbach, P., Laubach, S., Hartick, M., Kankleit, E., Keck, B., Menningen, M., Sielemann, R.: *Phys. Rev. Lett.* **64**, 1274 (1990)
15. Gunnlaugsson, H.P., Weyer, G., Dietrich, M., Fanciulli, M., Bharuth-Ram, K., Sielemann, R., ISOLDE Collaboration: *Appl. Phys. Lett.* **80**, 2657–2659 (2002)
16. Yoshida, Y., Kobayashi, Y., Yukihiro, K., Hayakawa, K., Suzuki, K., Yoshida, A., Ueno, H., Yoshimi, A., Shimada, K., Nagae, D., Asahi, K., Langouche, G.: *Physica B* **401–402**, 101–104 (2007)



17. Langouche, G., Yoshida, Y.: Nuclear methods to study defects and impurities in Si materials. In: Yoshida, Y., Langouche, G. (eds.) *Defects and Impurities in Silicon Materials- An Introduction to Atomic-Level Silicon Engineering*, chap. 8, p. 373. Springer (2016). In *Lecture Note in Physics*. doi:[10.1007/978-4-431-55800-2](https://doi.org/10.1007/978-4-431-55800-2)
18. Yoshida, Y., Hayakawa, K., Yukihiro, K., Ichino, M., Akiyama, Y., Kumabe, H., Soejima, H.: Development and applications of Mössbauer cameras. *Hyperfine Interact.* **198**, 23–29 (2010)
19. Ino, Y., Soejima, H., Hayakawa, K., Yukihiro, K., Tanaka, K., Fujita, H., Watanabe, T., Ogai, K., Moriguchi, K., Harada, Y., Yoshida, Y.: 3D-Mössbauer spectroscopic microscope for mc-Si solar cell evaluation. *Hyperfine Interact.* **237**, 13 (2016)
20. Istratov, A.A., Hieslmair, H., Weber, E.R.: Iron and its complexes in silicon. *Appl. Phys. A* **69**, 13–44 (1999)
21. Wright, E., Coutinho, J., Oberg, S., Torres, V.J.B.: *J. Appl. Phys.* **119**, 181509 (2016). doi:[10.1063/1.4948243](https://doi.org/10.1063/1.4948243)